ACTA METALLURGICA SLOVACA
2023, VOL. 29, NO. 1, 44-49

RESEARCH PAPER

# HIGH ENTROPY COATING FROM AlCoCrCuFeNi ALLOY, OBTAINED BY LASER ALLOYING

*Vasyl' Girzhon*[1], *Vladyslav Yemelianchenko*[2], *Oleksandr Smolyakov*[2]

[1] National University "Zaporizhzhya Polytechnic", 64 Zhukovsky Str., Zaporizhzhya, 69063, Ukraine
[2] Zaporizhzhya National University, 66 Zhukovsky Str., Zaporizhzhya, 69600, Ukraine.

*Corresponding author: emelyanchenkovlad@gmail.com, tel.: +380973247590, Department of General and Applied Physics, Zaporizhzhya National University, 69600, Zaporizhzhya, Ukraine.

Received: 31.01.2023
Accepted: 21.03.2023

## ABSTRACT

The influence of cooling rates and aluminum content on the phase composition of Al-Co-Cr-Cu-Fe-Ni system high-entropy alloy obtained by laser alloying of technically pure aluminium surface layers was investigated by XRD, EDX and metallographic analyses. It is shown that in the process of laser alloying the formation of an ordered multicomponent substitution solid solution based on BCC lattice took place, which is typical for high-entropy alloys. The process of high-entropy alloys AlCoCrCuFeNi and $Al_3$CoCrCuFeNi heterogeneous crystallization was modelled taking into account melt cooling rates. It is established that the formation of the obtained structure is a consequence of high melt cooling rates and high aluminum content in the laser alloying zone. The microhardness of the alloyed surface was higher compared to high-entropy alloys of this system obtained under equilibrium conditions and was equal to 6.59 GPa. Additional reasons that may affect the high microhardness values are analyzed.

**Keywords:** high–entropy alloys, laser alloying, rapid solidification, phase composition

## INTRODUCTION

Aluminum alloys are structural materials that are widely used in industry due to the optimal combination of physical, mechanical and chemical properties (low density, high specific strength, corrosion resistance, etc.). However, these alloys have a number of disadvantages, in particular the relatively low hardness and strength, which limit their use. Therefore, the urgent task is to develop and apply technological methods of processing, primarily surface, which would improve the mechanical and operational properties of these alloys [1]. Traditional methods of aluminum surface layers strengthening, such as anodizing and heat treatment, have a number of disadvantages, including high energy consumption, long duration and low productivity [2].

A promising area for improving the mechanical properties of the aluminum alloys surface layers is the use of methods which applies laser radiation, in particular laser alloying. The advantages of laser alloying include the simplicity of energy supply to the processing site, the ability to obtain layers with high hardness and wear resistance, modified to a depth of several micrometers to several millimeters; obtaining structures with high dispersion and minimal thermal impact zone; high adhesion between the coating and the matrix material, etc. [3, 4]. The melt high cooling rates ($10^3$… $10^6$ K/s), which are characteristic for this method, help to reduce the components segregation and prevent the nucleation and growth of brittle intermetallic compounds [5, 6]. An example of the laser alloying effective use to improve the mechanical properties of the aluminum alloys surface can be the creation of coatings containing quasicrystalline phases, which are characterized by high values of microhardness [7, 8].

Potential candidates for the role of material for these coatings are high-entropy alloys (HEAs), characterized by high hardness, corrosion resistance and high wear resistance [9]. HEAs typically consist of five or more components taken in an equiatomic (or close to equiatomic) ratio. A characteristic feature of this class of alloys is the presence in their phase composition of one or more multicomponent substitution solid solutions based on simple highly symmetric BCC, FCC or HCP lattices [10].

A small number of scientific publications on the production of HEAs by laser alloying, as well as detailed studies of the melt cooling rate influence on the processes of their structure formation, indicates that this issue requires further study. Therefore, the aim of this work is to analyze the Al-Co-Cr-Cu-Fe-Ni high-entropy alloys phase formation processes, taking into account the heterogeneous crystallization and the cooling rates, typical for laser alloying.

## MATERIAL AND METHODS

Alloying was performed on a pulsed YAG laser ($\lambda$ = 1.06 μm) in a protective argon atmosphere at a radiation density of 1 GW/m$^2$ and a pulse repetition frequency $\nu$ = 2 Hz, laser spots overlap was 30%. Samples of technically pure aluminum, similar in composition to Aluminum 1080, Aluminum 1080A (USA) and ENAW-1080A (EU), were selected as the matrix (the alloying object). Samples for laser alloying were cut in the form of parallelepipeds with side dimensions of 10x10x5 mm (plane parallel). Before applying alloying components to the samples surface, it was polished using abrasive paper with a particle size of 15 to 20 μm. After polishing, abrasive particles and metal residues on the surface were removed using ethyl alcohol. The alloying components were an equiatomic mixture of Co, Cr, Fe, Cu and Ni powders with a fraction size not exceeding 50 μm. The thickness of the coating was 150 μm. The phase composition was determined by XRD method using Bragg-Brentano focusing on a RIGAKU MINIFLEX 600 diffractometer (CuKα - radiation). The samples were examined in the range of angles 20º...120º according to the modes: U=30 kV, I=15 mA, scanning

step 0,1°. The microstructure of alloyed layers was studied using a TESCAN VEGA 3 scanning electron microscope equipped with an energy dispersive analysis (EDS) system, which made it possible to conduct a local chemical analysis of individual areas and establish the chemical components distribution along the laser alloying zone. The samples microhardness was measured by the Vickers method, a diamond pyramid with a square base and an angle at the top between opposite faces equal to 136˚ was used as an indenter. The working load was determined experimentally and consisted of 20 g for tested samples.

## RESULTS AND DISCUSSION

According to XRD data, four phases were observed in the samples surface layers after laser alloying: two solid solutions based on BCC and FCC lattice, intermetallic $Al_{13}(Me)_4$ (Me - alloying components of the mixture) and matrix aluminum (Fig. 1, a). Note that the precisely determined lattice parameters of BCC and FCC phases (**Table 1**) actually coincided with the lattice parameters of multicomponent substitution solid solutions, the formation of which is typical for HEAs of this system [11].
The formation of BCC solid solution in the HEAs obtaining process of the Al-Co-Cr-Fe-Ni system by laser alloying was described earlier in [12]. The addition to such an alloy of copper should lead to the formation, in addition to the BCC solid solution, also a multicomponent solid solution based on the FCC lattice [13, 14]. According to [9], copper is a stabilizer of FCC phase, as it can form continuous solid solutions or binary intermetallics with FCC lattice with other alloy components.
The formation of intermetallic $Al_{13}(Me)_4$ is typical for the phase formation processes of aluminum alloys at high cooling rates [12]. Note that the main alloying elements in the lattice of the intermetallic $Al_{13}(Me)_4$ may be iron and cobalt, because the solubility of chromium and nickel in the lattice of this type is lower. The solubility of copper is also low and is close to 6% at. [15].

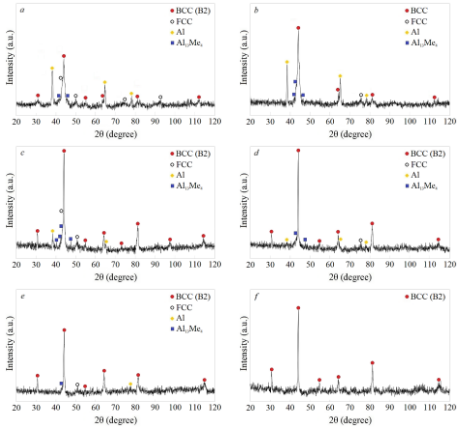


**Fig. 1** Diffractograms from the surface layers of aluminum samples after laser alloying with an equiatomic mixture of powders Co, Cr, Fe, Cu and Ni:

a) Alloying with a coating thickness of 150 μm.
b) Remelting of the alloyed surface
c) Re-alloying with a coating thickness of 150 μm.
d) Remelting of the alloyed surface
e) Re-alloying with a coating thickness of 80 μm.
f) Remelting of the alloyed surface

EDX analysis of the sample alloyed surface (**Fig. 2**) showed that the alloy components distribution on the LAZ surface is homogeneous except for aluminum and copper. Increased copper content was observed in the peripheral areas of LAZ, while increased aluminum content was present in the central areas of LAZ. This distribution of components can be related both to the difference between their melting temperatures and the influence of Marangoni-Gibbs effect [16]. It is known [17] that the FCC phase formed in this system is enriched in copper. Therefore, it can be assumed that its formation took place mainly in areas of LAZ with high copper content, i.e. in the peripheral areas of LAZ.
In order to equalize the chemical composition of LAZ, the alloy surface was subsequently remelted. This treatment led to an increase in the volume fraction of BCC phase and a decrease in the proportion of FCC phase in LAZ (Fig. 1, b). Such a change in the volume fractions of BCC and FCC phases can be caused by the alignment of the chemical composition by the volume of LAZ, in particular the more uniform distribution of aluminum and copper. The redistribution of the alloying components content in the lattices of both solid solutions was indicated by the change in their parameters (**Table 1**).

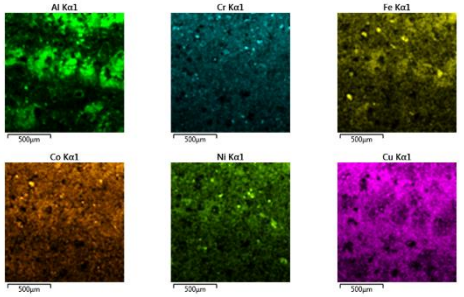


**Fig. 2** Distribution of chemical components on the top surface of LAZ

According to [18], the formation of ordered BCC and disordered FCC solid solutions is took place at an aluminum content in the alloy in the amount of 25… 40 at. %. However, in addition to solid solutions, matrix aluminum and aluminum-enriched $Al_{13}(Me)_4$ intermetallic were also present in the LAZ phase composition. This means that the alloyed layers chemical composition did not fully correspond to the homogeneity region of these solid solutions existence. To reduce the amount of aluminum in LAZ, re-alloying was performed, similar to the previous one. After such treatment, the surface layers phase composition did not change, but there was a decrease in the diffraction maxima intensities from the lattice of aluminum and intermetallic $Al_{13}(Me)_4$, which was the expected result (**Fig. 1**), c).
The distribution of the alloy components on the LAZ surface was similar to the distribution of the components after the initial alloying. The new remelting of the surface led to a decrease in the diffraction maxima intensities from the lattice of FCC solid solution, matrix aluminum and intermetallic $Al_{13}(Me)_4$ (Fig. 1, d).
The presence of reflections from the lattice of pure aluminum in LAZ indicated its excess. To reduce the amount of aluminum, another alloying with a backcoat thickness of 80 μm was performed. After such treatment, reflections from the BCC solid solution and traces of reflections from the lattice of the FCC solid solution were observed from the samples surface layers. There was a noticeable decrease in the volume fraction of aluminum and intermetallic $Al_{13}(Me)_4$ (Fig. 1, e).
The remelting of such a surface led to the forming in the alloyed layers of only one BCC phase (Fig. 1, f) with a slightly higher

parameter than after the first alloying. The reason for this change in the parameter may be an increase in the aluminum content in the BCC phase (**Table 1**).

It should be noted that the structural changes caused by alloying led to an increase in the microhardness values of the samples surface layers (**Table 1**). The constant increase in the values of microhardness can be explained by a gradual decrease in the volume fraction of matrix aluminum and an increase in the volume fraction of BCC solid solution. Characteristically, the microhardness of the last sample is higher than that of high-entropy alloys of this system obtained under equilibrium conditions [17]. An additional reason for the high values of microhardness in this case may be the high degree of structure dispersion typical for alloys obtained at high melt cooling rates.

The experimentally obtained results, which indicated that the amount of FCC phase decreased along with the amount of aluminum in the LAZ (until its disappearance), required the explanation. In our opinion, one of the possible reasons for this may be the high cooling rates of the melt during pulsed laser surfaces alloying. To establish the influence of cooling rates on the alloyed layers phase composition, the crystallization process of high-entropy alloys AlCoCrCuFeNi and $Al_3CoCrCuFeNi$ was modeled.

**Table 1** Phase composition of LAZ, parameters of the lattice of solid solutions and microhardness of alloyed surfaces

| Type of treatment | Phase composition | Lattice parameters, nm | | Microhardness, GPa |
|---|---|---|---|---|
| Alloying with a coating thickness of 150 μm. | BCC (B2) FCC Al $Al_{13}Me_4$ | BCC | 2,8838±0,0007 | 3,33 |
| | | FCC | 3,6022±0,0016 | |
| Remelting of the alloyed surface | BCC (B2) FCC Al $Al_{13}Me_4$ | BCC | 2,8685±0,0007 | 3,73 |
| | | FCC | 3,5726±0,0016 | |
| Re-alloying with a coating thickness of 150 μm. | BCC (B2) FCC Al $Al_{13}Me_4$ | BCC | 2,8887±0,0007 | 3,99 |
| | | FCC | 3,6068±0,00027 | |
| Remelting of the alloyed surface | BCC (B2) FCC Al $Al_{13}Me_4$ | BCC | 2,8718±0,0007 | 4,72 |
| | | FCC | 3,6002±0,00016 | |
| Re-alloying with a coating thickness of 80 μm. | BCC (B2) FCC Al $Al_{13}Me_4$ | BCC | 2,8970±0,0007 | 4,75 |
| | | FCC | 3,5805±0,00016 | |
| Remelting of the alloyed surface | BCC (B2) | BCC | 2,8945±0,0007 | 6,59 |

In the case of forming the surface layers structure during laser alloying, it is advisable to consider heterogeneous crystallization as the main, as active centers of crystallization can be both matrix material and a significant amount of impurities formed during combustion of binder, oxide films etc.. Therefore, the numerical calculation of the volume fraction proportion was performed using the equations

$$\Delta X(t_i) = -\exp\left[-\left(\frac{\pi}{3} IU^3(t-\tau)^4 + \frac{4\pi}{3} NU^3 t^3\right)\right]\left(-\frac{4\pi}{3} IU^3(t-\tau)^3 - 4\pi NU^3 t^2\right)\Delta t \quad (1.)$$

$$X = \sum \Delta X(t_i) \quad (2.)$$

obtained from the equation [19]:

$$X(t) = 1 - \exp\left[-\left(\frac{\pi}{3} IU^3(t-\tau)^4 + \frac{4\pi}{3} NU^3 t^3\right)\right] \quad (3.)$$

where $I$ and $U$ are the rates of crystals nucleation and growth, respectively;

$X$ is the crystallized volume fraction; $N$ is the density of heterogeneous crystallization centers per unit volume; $\tau$ is the critical time of nucleation;

$t_i = t_i\text{-}1 + \Delta t$.

The equations [20] were used to calculate the rates of nucleation and growth of crystals:

$$I(T) = \frac{N_0 D}{a_0^2} \exp\left(-\frac{16\pi\sigma^3 V_m^2}{3kT\Delta G^2}\right) \quad (4.)$$

$$U(T) = \frac{D}{a_0}\left[1 - \exp\left(-\frac{\Delta G}{RT}\right)\right] \quad (5.)$$

where $N_0$ is the number of atoms per unit volume; $a_0$ is the atomic jump distance, calculated as $\sum c_i d_i$ ; $d_i$ is the atomic diameter of the $i$-th component, $c_i$ is the atomic fraction of the $i$-th element; $D$ is the diffusion coefficient; $k$ is the Boltzmann constant; $\sigma$ – solid-liquid interface energy; $V_m$ is the molar volume calculated as $\sum c_i V_m^i$ , the molar volume of the $i$-th element, $c_i$ is the atomic fraction of the $i$-th element; $\Delta G$ is the difference of Gibbs free energies. The number of atoms per unit volume of BCC and FCC solid solutions was defined as:

$$N_0^{BCC} = \frac{2}{a_{BCC}^3} \quad (6.)$$

$$N_0^{FCC} = \frac{4}{a_{FCC}^3} \quad (7.)$$

where $a_{BCC}$ and $a_{FCC}$ are the parameters of BCC and FCC phases, respectively. Values of thermodynamic driving force were calculated in the Thomson-Speypen approximation, developed for metal alloys [21]:

$$\Delta G(T) = \frac{2\Delta H_m T(T_m - T)}{T_m(T_m + T)} \quad (8.)$$

where $\Delta H_m$ is the enthalpy of fusion, calculated as $\sum c_i \Delta H_m^i$, $\Delta H_m^i$ - the enthalpy of fusion of the $i$-th element, $c_i$ - the atomic fraction of the $i$-th element; $T_m$ - melting point. The diffusion coefficients in the first approximation were calculated by the Arrhenius formula:

$$D = D_0 \exp\left(-\frac{Q}{RT}\right) \quad (9.)$$

where $D_0$ is the coefficient (pre-exponential factor), $Q$ is the activation energy.

The melt cooling rate in the calculations according to formulas (1) - (9) was taken into account as follows: the temperature varied in steps of 1 K, and $\Delta t$ was chosen numerically equal to $1/v$ ($v$ is the cooling rate). Appropriate calculations were performed for cooling rates of $10^3$… $10^5$ K/s. These cooling rates are typical for metal alloys pulsed laser processing on YAG lasers [5, 6, 22].

The following numerical values were used for the calculations: density of crystallization centers $N = 10^{19}$ m$^{-3}$ [19]; coefficient (pre-exponential factor) $D_0 = 3 \cdot 10^{-7}$ m$^2$/s [23]; activation energy $Q$ = 166 kJ/mol [24]; lattice parameters of solid solutions $a_{BCC}$ = 0.288 nm, $a_{FCC}$ = 0.360 nm [11]; solid-liquid interface energy $\sigma$ = 0.2 J/m$^2$ [25]. The temperature dependence of the critical nucleation time $\tau(T)$ was taken from [26]. The enthalpy of mixing, molar volume and atomic diameters of the components are given in **Table 2**.

According to the calculations, the crystallized volume fraction of the FCC phase during cooling of the aluminum-enriched alloy $Al_3CoCrCuFeNi$ at a rate of $10^5$ K/s is about 9.8% (**Fig. 3**, *a*). Decreasing the cooling rate of the melt leads to an increase in the volume fraction of the FCC phase. Thus, at a cooling rate of $10^4$ K/s it is 45.6% (Fig. 3, *b*), and at a cooling rate of $10^3$ K/s - 48.7% (Fig. 3, *c*). Calculated on the basis of the results from [22] the cooling rate for this laser, depending on the type of irradiated alloy, can be $10^3$… $10^5$ K/s. Since, according to XRD analysis, the volume fraction of FCC phase in alloyed layers was insignificant, and the thermal conductivity of matrix aluminum is higher than that of alloys based on ferrous metals, we can assume that the cooling rate in the alloying process was close to $10^5$ K/s.

**Table 2** Values of enthalpy of mixing, molar volume and atomic diameters for alloy components [27]

| Alloy component | $\Delta H_m^i$, kJ/mol | $V_m^i$, m$^3$/mol | $d_i$, m |
|---|---|---|---|
| Al | 10,7 | $1 \cdot 10^{-5}$ | $2{,}86 \cdot 10^{-10}$ |
| Co | 16,2 | $6{,}7 \cdot 10^{-6}$ | $2{,}5 \cdot 10^{-10}$ |
| Cr | 20,5 | $7{,}23 \cdot 10^{-6}$ | $2{,}49 \cdot 10^{-10}$ |
| Cu | 13,1 | $7{,}1 \cdot 10^{-6}$ | $2{,}55 \cdot 10^{-10}$ |
| Fe | 13,8 | $7{,}1 \cdot 10^{-6}$ | $2{,}47 \cdot 10^{-10}$ |
| Ni | 17,2 | $6{,}6 \cdot 10^{-6}$ | $2{,}49 \cdot 10^{-10}$ |

Decreasing the aluminum content leads to a decrease in the proportion of FCC phase crystallized volume. Thus, in the equiatomic alloy AlCoCrCuFeNi at the cooling rate of the melt $10^5$ K/s there is no formation of FCC phase observed (**Fig. 4**, a).

The FCC phase volume fractions at cooling rates of $10^4$ K/s and $10^3$ K/s are about 43.4% and 48.3%, respectively (Fig. 4, *b*, *c*). Step-by-step calculations of crystallized volume fraction with a change in the melt cooling rate in the range $10^5$…$10^4$ K/s allowed to establish the critical rate at which complete inhibition of the FCC solid solution formation occurs. It turned out to be equal to $6 \cdot 10^4$ K/s (**Fig. 5**). The obtained results are consistent with the known experimental data, according to which the presence of FCC solid solution is not observed in the alloy AlCoCrCuFeNi at the cooling rates of the melt $10^5$ K/s [13, 14].

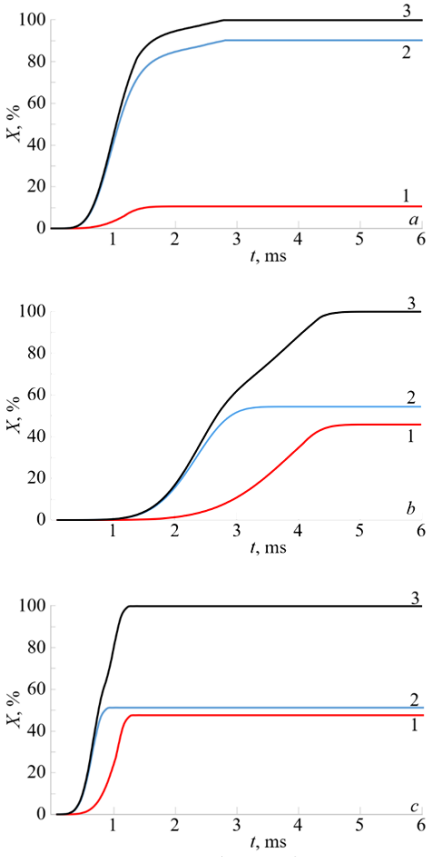


**Fig. 3.** Crystallized volume fraction of FCC- (1) and BCC (2) phases and total fraction of crystallized volume (3) in $Al_3CoCrCuFeNi$ alloy at melt cooling rates $10^5$ K/s (a), $10^4$ K/s (b) and $10^3$ K/s (c).

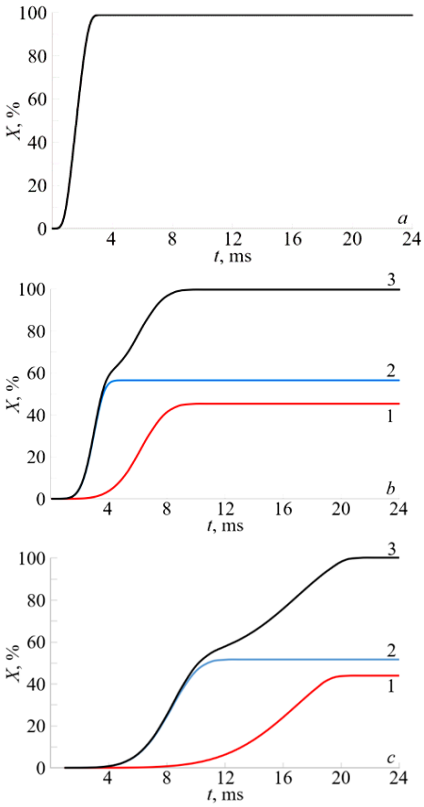


**Fig. 4** Crystallized volume fraction of FCC- (1) and BCC (2) phases and total fraction of crystallized volume (3) in AlCoCrCuFeNi alloy at melt cooling rates $10^5$ K/s (*a*), $10^4$ K/s (*b*) and $10^3$ K/s (*c*).

Therefore, according to the calculations, the decrease in the aluminum content in LAZ leads to a decrease in the amount of FCC solid solution, which was observed experimentally (**Fig. 1**).
It should be noted that the density of the heterogeneous crystallization centers per unit volume can have a significant effect on the ratio between the volume fractions of FCC and BCC solid solutions. The above calculations were performed at $N = 10^{19}$ m$^{-3}$, given in [19]. Increasing of the heterogeneous crystallization centers density ($N = 10^{20}$ m$^{-3}$) leads to an increase in the FCC phase fraction, and, as a consequence, to the discrepancy between theoretical and experimental results. With a decrease in the heterogeneous crystallization centers density ($N = 10^{18}$ m$^{-3}$), a decrease in the FCC phase volume fraction is observed (**Table 3**). The obtained calculations allow us to state that the FCC phase crystallization process takes place mainly by a heterogeneous mechanism, because in the absence of heterogeneous nucleation at a melt cooling rate of about $10^4$ K/s only BCC solid solution would be formed. The calculations of the critical nucleation time for multicomponent substitution solid solutions also indicate the heterogeneous nature of the FCC phase formation [26].

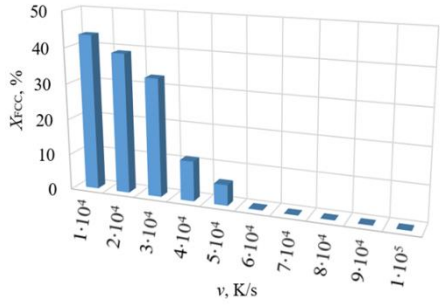


**Fig. 5** Crystallized fraction of FCC phase in AlCoCrCuFeNi alloy at different melt cooling rates

Thus, the melt cooling rate and the presence of heterogeneous crystallization centers have a significant impact on the processes of HEAs phase formation during laser alloying, which as a result makes it possible to obtain coatings with high mechanical properties.

**Table 3** The crystallized volume fractions of FCC and BCC phases at the cooling rate of the melt $10^5$ K/s at different values of the density of the centers of heterogeneous crystallization

| Alloy | $N = 10^{18}$ m$^{-3}$ | $N = 10^{19}$ m$^{-3}$ | $N = 10^{20}$ m$^{-3}$ |
|---|---|---|---|
| AlCoCrCuFeNi | $X_{FCC}$ = 0%<br>$X_{BCC}$ = 100% | $X_{FCC}$ = 0%<br>$X_{BCC}$ = 100% | $X_{FCC}$ = 8,07%<br>$X_{BCC}$ = 91,93% |
| $Al_3$CoCrCuFeNi | $X_{FCC}$ = 2,08%<br>$X_{BCC}$ = 97,91% | $X_{FCC}$ = 9,78%<br>$X_{BCC}$ = 90,23% | $X_{FCC}$ = 36,74%<br>$X_{BCC}$ = 63,26% |

## CONCLUSIONS

In the work, an experimental study of the phase composition, microstructure, and mechanical properties of Al-Co-Cr-Cu-Fe-Ni system HEAs, obtained by laser alloying method on the surface of technically pure aluminum, and crystallization processes modeling was carried out. The obtained scientific results and the established physical regularities are of practical interest in the creation of methodological and scientific foundations for the development of high-entropy alloys for purposeful management of their structure and properties, as well as the practical use of this class of alloys - the creation of protective coatings on products from industrial alloys in local places with high degree of adhesion.

1. Laser alloying of aluminum with an equiatomic mixture of powders Co, Cr, Fe, Cu and Ni due to high cooling rates of the melt inhibits the formation of FCC solid solution, which allows to obtain a single-phase HEA coating with BCC structure.
2. The presence of only one BCC phase and a high degree of dispersion of the structure in the lazer alloying zone leads to an increase in microhardness to 6.59 GPa.
3. It was shown for the first time that the aluminum content decrease in alloys of the Al-Co-Cr-Cu-Fe-Ni system leads to a decrease in the FCC phase crystallized volume fraction, in contrast to alloys of the Al-Co-Cr-Fe-Ni system, in which the share of FCC phase increases with decreasing aluminum content.

4. For the first time, a correlation between the density of heterogeneous crystallization centers and the volume fraction of the FCC phase in alloys of the Al-Co-Cr-Cu-Fe-Ni system was established theoretically.

**ACKNOWLEDGMENTS:**
Authors would like to acknowledge doctor of science Sklyarchuk V. M., Physics Department Chief Researcher, Ivan Franko National University of Lviv for his help in discussing and interpreting the results.

## REFERENCES

1. N. Gao: *Aluminium alloys*, second ed., Mdpi Ag., Basel, 2008.
2. M. Ardelean, S. Lascău, E. Ardelean, A. Josan: IOP Conference Series: Materials Science and Engineering, 294, 2018, 012042. https://doi.org/10.1088/1757-899X/294/1/012042.
3. V.V. Girzhon, I. V. Tantsyura: Metallophysics and Advanced Technologies', 28, 2006, 1249-1259.
4. J.M. Poate, G. Foti, D.C. Jacobson: *Surface Modification and Alloying: by Laser, Ion, and Electron Beams*, Springer Science & Business Media, New York;, 2013.
5. H. Zhang, Y.Z. He, X.M. Yuan, Y. Pan: Applied Surface Science, 256 (20), 2010, 5837-5842. https://doi.org/10.1016/j.apsusc.2010.03.056.
6. H. Assadi, S. Reutzel, D.M. Herlach: Acta Materialia, 54 (10), 2006, 2793-2800. https://doi.org/10.1016/j.actamat.2006.02.018.
7. K. Biswas, R. Galun, B. L Mordike, K. Chattopadhyay: Journal of Non-Crystalline Solids, 334, 2004, 517-523. https://doi.org/10.1016/j.jnoncrysol.2003.12.034.
8. V. V. Girzhon, O. V. Smolyakov, I. V. Tantsyura: The Physics of Metals and Metallography, 106, 2008, 384-388. https://doi.org/10.1134/S0031918X08100086.
9. B.S. Murty, J.W. Yeh, S. Ranganathan, P.P. Bhattacharjee: *High-Entropy Alloys*, second ed., Elsevier, 2019.
10. Y. Zhang: *High-Entropy Materials A Brief Introduction*, Springer, Singapore, 2019. https://doi.org/10.1007/978-981-13-8526-1.
11. M. V. Karpets, O. M. Myslyvchenko, O. S. Makarenko, M. O. Krapivka, V. F .Gorban': Problems of friction and wear, 63, 2014, 103-111.
12. V. V. Girzhon, V. V. Yemelianchenko, O. V. Smolyakov: Metallophysics and Advanced Technologies, 43, 2021, 399–406. https://doi.org/10.15407/mfint.43.03.0399.
13. S. Singh, N. Wanderka, B.S. Murty, U. Glatzel, J. Banhart: Acta Materialia, 59 (1), 2011, 182-190. https://doi.org/10.1016/j.actamat.2010.09.023.
14. M.V. Ivchenko, V.G.Pushin, N. Wanderka: Technical Physics, 59, 2014, 211-223.
15. B. Grushko, Ch. Freiburg: Journal of Materials Research, 7, 1992, 1100-1103. https://doi.org/10.1557/JMR.1992.1100.
16. J.M. Wang, G.H. Liu, Y.L. Fang, W.K Li: Reviews in Chemical Engineering, 32, 2016, 551-585. https://doi.org/10.1515/revce-2015-0067.
17. C. C. Tung, J. W. Yeh, T. T. Shun, S. K. Chen, Y. S. Huang, H. C. Chen: Materials Letters, 61, 2007, 1–5. https://doi.org/10.1016/j.matlet.2006.03.140.
18. I. S. Aristeidakis, M.-I. T. Tzini: *High Entropy Alloys*, Volos, 2016.
19. D.R.Uhlman: Journal of Non-Crystalline Solids, 7, 1978, 337-348.
20. D Kristian: *Teorija prevrashhenij v metallah i splavah*, Mir, Moskow, 1978.
21. C.V. Thomson, F. Spaepen: Acta Metallurgica, 27, 1979, 1855-1859.
22. D.I. Anpilogov, V.V. Girzhon: Ukrainian Journal of Physics, 42, 1997, 301-304.
23. V.N. Yeremenko, Y.V. Natanzon, V.I. Dybkov: Journal of the Less Common Metals, 50, 1976, 29 – 48.
24. S. Rohila, R.B. Mane, S. Naskar, B.B. Panigrahi: Materials Letters, 256, 2019, 126668. https://doi.org/10.1016/j.matlet.2019.126668.
25. Z. Jian, K. Kuribayashi, W. Jie: Materials Transactions, 43, 2002, 721-726. https://doi.org/10.2320/matertrans.43.721.
26. V.V. Girzhon, V.V. Yemelianchenko, O.V. Smolyakov, A.S. Razzokov: Results in Materials, 15, 2022, 100311. https://doi.org/10.1016/j.rinma.2022.100311.
27. [08.09.2022], http://www.webelements.com/